Electromagnetic Deposition in an Anatomically Based Model of Man for Leakage Fields of a Parallel-Plate Dielectric Heater

JIN-YUAN CHEN, STUDENT MEMBER, IEEE, AND OM P. GANDHI, FELLOW, IEEE

Abstract —**The three-dimensional finite-difference time-domain (FDTD) method has been used to calculate the local layer-averaged and whole-body-averaged specific absorption rates (*SAR*'s) and internal RF currents in a 5628-cell anatomically based model of man for spatially variable electromagnetic fields of a parallel-plate applicator representative of RF dielectric heaters used in industry. Included in the calculations are the shape and dimensions of the applicator plates as well as a typical spacing of 21 cm to the human operator. The calculated leakage fields are in agreement with the experimentally measured values. The conditions of exposure of the man model considered are: isolated from ground, feet in contact with ground, and an additional grounded top plate 13.1 cm above the head to simulate screen rooms that are occasionally used for RF heaters. Also considered is the model with a separation layer of rubber ($\epsilon_r = 4.2$) of thickness 2.62 cm between feet and ground to simulate the shoe-wearing condition. For peak *E* fields as high as 1000–2700 V/m that have been measured at the locations of the operator, significant internal RF currents on the order of 0.5–2.3 A are projected for the operator. Laboratory measurements of the foot currents at 27.12 and 40.68 MHz for a human subject are in agreement with the calculated values.**

I. Introduction

RF DIELECTRIC heaters operating typically at the ISM frequencies of 13.56, 27.12 or 40.68 MHz are used in industry for a variety of dielectric heating applications. Some of the typical uses are sealing or welding of plastics, drying glue to join pieces of wood, curing particle boards, etc. [1]. Depending upon the materials that are to be processed, the output power of the heaters may range from a few hundred watts to tens of kilowatts. The material heating is obtained by using shaped parallel-plate electrodes forming a capacitor-type applicator for RF power. Significant leakage electric (E) and magnetic (H) fields with values as high as 1000–2700 V/m and 1–5 A/m, respectively, have been measured at the location of the operators of RF dielectric heaters [2], [3]. These fields are considerably in excess of even the most lax of the RF safety guidelines used anywhere in the world. By one estimate, over 40 000 workers are exposed in the United States alone to the leakage fields from the RF dielectric heaters [1].

Manuscript received February 16, 1988; revised July 29, 1988. This work was supported by the National Institute of Environmental Health Sciences under Grant ES 03329.

The authors are with the Department of Electrical Engineering, University of Utah, Salt Lake City, UT 84112.

IEEE Log Number 8824253.

In the past we have tried to examine the coupling of electromagnetic fields to an inhomogeneous model representation of the human body for near-field irradiation conditions [4]. We have also attempted to characterize the magnitudes of the RF currents that flow through the operator's feet while working with some typical dielectric heaters [5]. In previous work [4] a relatively crude 180-cell model representation of the human body could only be used because the method of moment (MOM) procedure used at that time used the matrix-inversion technique for which the computational time requirements increased rapidly as N^3, where N is the number of cells. Also, the plane-wave-spectrum approach that was used to characterize the incident fields was not flexible enough to permit a detailed modeling of the applicator and the surrounding boundaries. Similarly, while we have characterized the magnitudes of the RF currents through the feet [5], no information is available on the distribution of currents induced in the body, particularly the torso, which is closest to the parallel-plate applicator that is the source of the leakage fields.

We have recently developed the finite-difference time-domain method for bioelectromagnetic dosimetry problems and have used it for calculations of specific absorption rates (*SAR*'s) for anatomically based models of a human being for far-field irradiation conditions [6], [7] and for near fields of multiaperture or multidipole annular phased arrays used for hyperthermia [8]. In this paper we present the results for the *SAR* and current distributions for a 5628-cell model of a human being subjected to the leakage fields of a parallel-plate applicator with dimensions that are typical of heaters used for plastic sealers. Grounded and ungrounded conditions are used for the anatomically based model. To simulate screen rooms that are occasionally used for the RF sealers, an upper grounded plate is used for some of the calculations. The calculated results are compared with some of the experimental data that have been obtained.

II. Description of the Method and the Model

The finite-difference time-domain (FDTD) method was first proposed by Yee [9] and later developed by Taflove *et al.* [10]–[12], Holland [13] and Kunz and Lee [14]. As

0018-9480/89/0100-0174$01.00

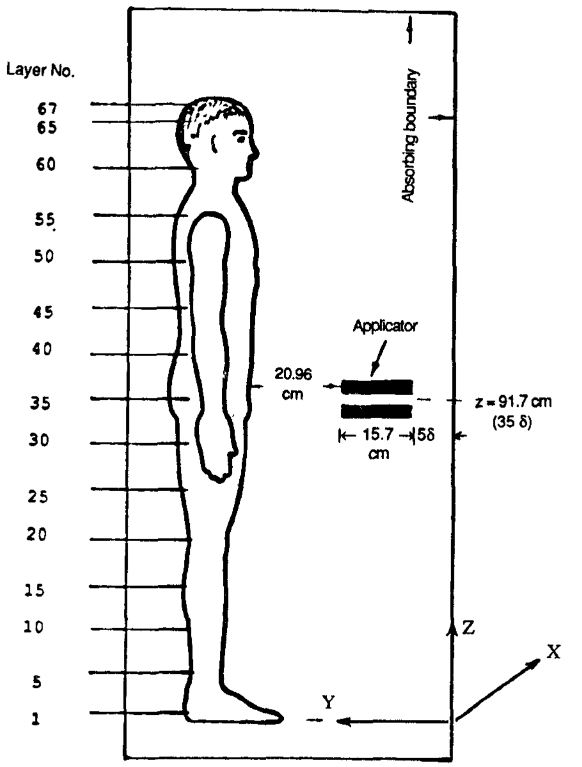

Fig. 1. Geometry of the applicator and man model. The separation between each of the layers is $\delta = 2.62$ cm.

aforementioned, we have recently used it for bioelectromagnetic problems [6]–[8]. In this method, described in detail in [6]–[8], the coupled Maxwell's equations in the differential form are solved for various points of the scatterer as well as its surroundings in a time-stepped manner until converged solutions are obtained. To ensure stability, the time step δt is given by $\delta/2v$, where δ is the cell size and v the maximum velocity of the electromagnetic (EM) wave encountered anywhere in the modeled space which includes the human model, the intervening space, the applicator, and the surroundings. For our application $v = c$ which is the velocity of the EM wave in air. The entire modeled space is divided into cubical cells with the cell size δ which should be smaller than or equal to one-tenth of the smallest wavelength of EM energy encountered anywhere in the modeled space. This would imply a cell size $\delta \leqslant \lambda_\epsilon/10$ where λ_ϵ is the wavelength at the irradiation frequency in high-water-content tissue such as muscle. Since the modeled space must be restricted in size because of the computer limitations, absorption boundary conditions are therefore used at the boundaries of the modeled space to simulate radiation into space.

A sectional view of the geometry of the modeled space is shown in Fig. 1. Consistent with the inhomogeneous, anatomically based model of the human being [7], a cell size of 2.62 cm is used to subdivide the total interaction volume of Fig. 1, which yields a total of $36 \times 32 \times 82$ or 94 464 cells. To simulate an RF sealer, a parallel-plate applicator of dimensions 57.64×15.72 cm ($22\delta \times 6\delta$) with an interplate separation of 2.62 cm and a thickness for each of the metallic plates of 2.62 cm is assumed as the leakage source at a distance of 20.96 cm (8δ). These dimensions are quite representative of the kind of RF sealers used in industry. The external absorbing boundaries are placed at a distance of 5–7δ (13.1–18.34 cm) on all sides of the man model except the head where a somewhat larger separation of 8δ is taken to allow placement of a top metallic plate (assumed grounded) for conditions where the whole system may be located in a screen room. For conditions of ground contact a metallic plate is assumed under the feet of the model. To reduce the modeled space it is desirable to bring the absorbing boundaries as close to the region of interest as possible. We have verified the adequacy of 5–7δ for separation from the absorbing boundaries by running a two-dimensional lossy slab model in the interaction space shown in Fig. 1. Results of the calculated *SAR* variation for 5δ separation from the absorbing boundaries were found to be within 5 percent of the values obtained for 10δ separations. Separations of 5δ have therefore been used for the absorbing boundaries from the outer edge of the parallel plates on one side and from the back of the human model on the other side. A separation of 7δ to the absorbing boundary has been used under the feet for conditions of remoteness from the ground or "isolated" exposure conditions. To simulate the shoe-wearing condition a separation layer of rubber ($\epsilon_r = 4.2$) that is one cell thick (2.62 cm) is assumed between the feet and the ground plane. This value of the dielectric constant has been estimated by measuring the equivalent capacitance of an electrical safety shoe (size 11, Vibram Manufacturing Company) with a Hewlett-Packard model 4815A vector impedance meter over the frequency range 0.5–60 MHz. Also $\epsilon_r = 4.2$ is close to the values given in reference handbooks for Neoprene rubber.

Similar to [6] and [7], the inhomogeneous model of the human body is taken from the book *A Cross-Section Anatomy* by Eycleshymer and Schoemaker [15]. This book contains cross-sectional diagrams of the human body which were obtained by making cross-sectional cuts at spacings of about one inch in human cadavers. The process for creating the data base of the man model was the following: first of all, a quarter-inch grid was taken for each single cross-sectional diagram and each cell on the grid was assigned a number corresponding to one of the 14 tissue types or air given in Table I. Thus the data associated with a particular layer consisted of three numbers for each square cell: x and y positions relative to some anatomical reference point in this layer, usually the center of the spinal cord; and an integer indicating which tissue that cell contained. Since the cross-sectional diagrams available in [15] are for somewhat variable separations typically 2.3–2.7 cm, a new set of equispaced layers was defined at 1/4-in intervals by interpolating the data onto these layers. Since the 1/4-in cell size is too small for the memory space of present-day computers, the proportion of each tissue type was calculated next for somewhat larger cells of 1-in size combining the data for $4 \times 4 \times 4 = 64$ cells of the smaller dimension. Without changes in the anatomy, this process allows some variability in the height and weight of the

TABLE I
DIELECTRIC CONSTANTS, CONDUCTIVITIES, AND MASS DENSITIES OF THE TISSUE TYPES USED IN CREATING THE HUMAN MODEL AT 27.12 AND 40.68 MHz

Tissue Type	27.12 MHz ϵ_r	27.12 MHz σ S/m	40 68 MHz ϵ_r	40 68 MHz σ S/m	mass density ρ Units of 1000 kG/m^3
Air	1.0	0.0	1 0	0.0	0.0012
Muscle	106	0.74	92	0.77	1.05
Fat, bone	29	0.04	22	0.04	1.20
Blood	102	0.28	93	0.48	1.00
Intestine	60	0 29	53	0.32	1.00
Cartilage	29	0 04	22	0 04	1 00
Liver	132	0 51	115	0 54	1.03
Kidney	209	0 79	170	0 84	1.02
Pancreas	206	0 69	175	0.74	1.03
Spleen	206	0.69	175	0.74	1.03
Lung*	34	0 17	31	0.20	0.33
Heart	210	0 64	164	0.66	1 03
Nerve, brain	155	0.45	132	0.46	1 05
Skin	106	0.74	92	0.77	1.00
Eye	155	0.45	132	0.46	1.00

* We have used 33 percent lung tissue and 67 percent air for the dielectric properties of the lung.

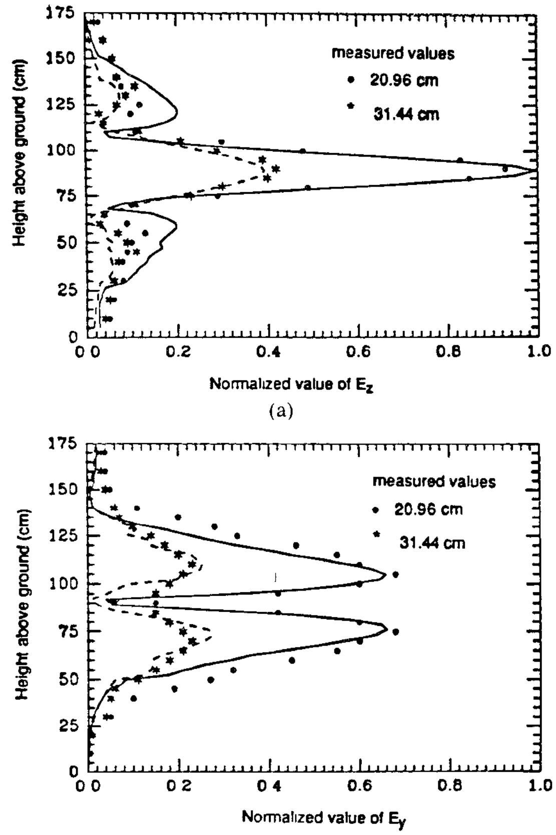

Fig. 2. Vertical and horizontal components of E field calculated (smooth curves) and measured for points along the central vertical axis ($x = 0$) in vertical planes at distances of 20.96 (8δ) and 31.44 cm (12δ) from the parallel-plate applicator. Frequency = 27.12 MHz. (a) Vertical component E_z. (b) Horizontal component E_y.

body. We have taken the final cell size of 2.62 cm (rather than 1 in or 2.54 cm) to obtain the whole-body weight of 69.6 kg for the model.

We have used the commonly used industrial heater frequencies of 27.12 and 40.68 MHz for all our calculations. The lower ISM frequency of 13.56 MHz has not been used for calculations since for comparable E and H fields the *SAR*'s would be considerably lower at this frequency. The dielectric constants and conductivities taken for the various tissues are given in Table I [16], [17].

The calculations are started with an initial sinusoidally varying electric field with uniform amplitude and phase assumed for all the cells in the parallel-plate applicator. A magnetic field of 1/377 of the electric fields is similarly taken for all the cells. The fields are calculated for all 94 464 cells with the various components of E and H fields calculated at points that are separated one-half cell distances apart in a given cell [6], [7]. Consistent with the requirement $\delta t = \delta/2c$, a time step of 4.367×10^{-11}s is taken for calculations at both 27.12 and 40.68 MHz. Converged solutions at all points of the interaction volume are obtained in interaction times typically on the order of three time periods of oscillation.

Iterations of 2500 and 1700 time steps have been found to be quite adequate to obtain the converged solutions at 27.12 and 40.68 MHz, respectively. The calculations have been made using CRAY XMP computer requiring CPU times of three to six minutes, depending upon the number of iterations.

III. TEST RUNS

A set of test runs has been made to obtain the field distributions from a parallel-plate applicator without the operator for a couple of vertical planes at distances of 20.96 (8δ) and 31.44 cm (12δ), respectively. For these calculations a ground plane was assumed at a distance of 89.1 cm underneath the lower plate of the applicator. The calculated vertical and horizontal E-field components and the total E field are shown in Figs. 2–4. These are compared with the measured values that were obtained using Holaday Industries model HI 3003 E-field probe. The relative magnitudes and spatial variations of the calculated fields are in excellent agreement with the measured values. The third field component E_x was considerably smaller than the other two components and hence has not been plotted nor compared with the experimental data. Similar agreements between calculated and measured variations of the E fields have also been obtained for 40.68 MHz.

IV. *SAR*'S AND INDUCED RF CURRENTS

Because of the time and spatial stepping in the FDTD calculations, the actual locations of the calculated E_x, E_y, and E_z are somewhat different and correspond to $(i+1/2, j, k)$, $(i, j+1/2, k)$ and $(i, j, k+1/2)$, respectively, for the (i, j, k) cell. Somewhat different values are

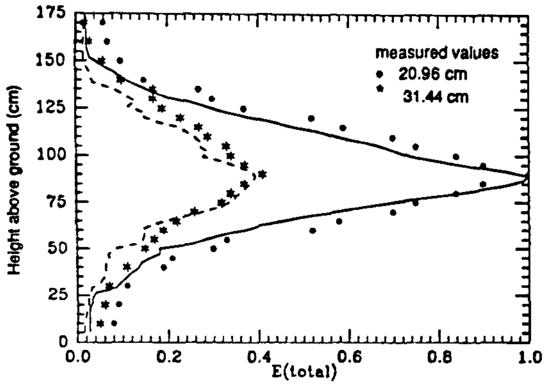

Fig. 3. The total electric field calculated (curves) and measured for points along the central vertical axis ($x=0$) in vertical planes at distances of 20.96 and 31.44 cm from the parallel-plate applicator. Frequency = 27.12 MHz.

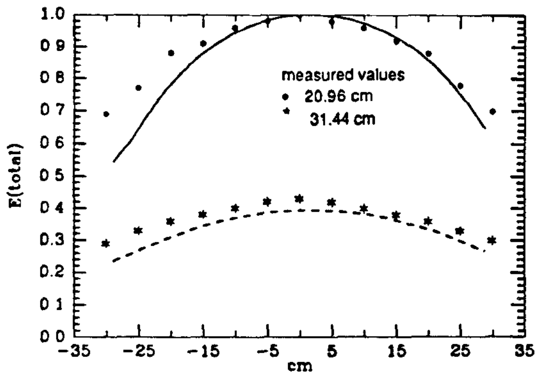

Fig. 4. The total electric field calculated (curves) and measured for points along the central horizontal axis ($z=35\delta=91.7$ cm) at distances of 20.96 and 31.44 cm from the parallel-plate applicator. Frequency = 27.12 MHz.

correspondingly involved for the various parameters such as ϵ, σ, and the mass density ρ. From converged solutions the SAR for the (i, j, k) cell is obtained from the equation:

$$SAR(i,j,k) = \sum_{x,y,z} \frac{\sigma_x(i,j,k)\left[E_{x,\max}(i,j,k)-E_{x,\min}(i,j,k)\right]^2}{8\rho_x(i,j,k)}. \quad (1)$$

The layer-averaged and whole-body-averaged SAR's are subsequently obtained by averaging over the corresponding local values of the SAR's. The layer-averaged SAR distributions calculated for a peak vertical electric field of 1 V/m (rms) measured anywhere for a vertical plane 20.96 cm in front of the parallel-plate applicator (generally the central point corresponding to maximum field in Fig. 2(a)) are shown in Figs. 5 and 6 for irradiation frequencies of 27.12 and 40.68 MHz, respectively. The whole-body-averaged SAR's for the various conditions of exposure of the model—isolated, shoe-wearing, grounded, and bottom ground and a grounded top plate 13.1 cm above the head (ground-topped)—are given in Table II for the two irradiation frequencies. The SAR's calculated for the grounded conditions are over two times higher than those for the isolated model (no ground underneath) conditions. Also somewhat higher SAR's still are calculated for conditions of exposure where a grounded top plate 13.1 cm above the head is used as well. It may be recalled that this condition has been studied since RF dielectric heaters are occasionally placed in screen rooms to prevent radiation into space. From Table II, the whole-body-averaged SAR's calculated for the rubber-sole shoe-wearing condition are 73.5 and

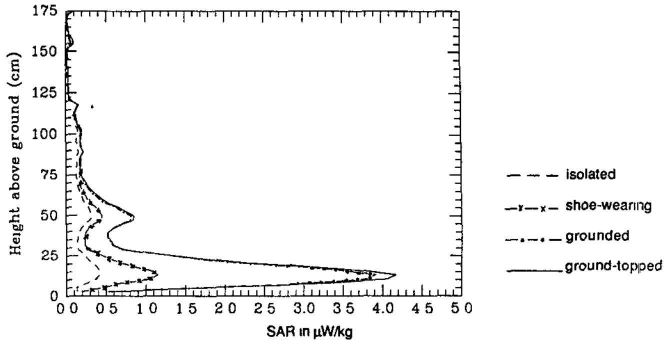

Fig. 5. Layer-averaged SAR distributions for an isolated, shoe-wearing, grounded, and ground-topped man model at 27.12 MHz under near-field exposure condition. Maximum $E_{\text{rms}}=1$ V/m at 21 cm in front of the parallel-plate applicator.

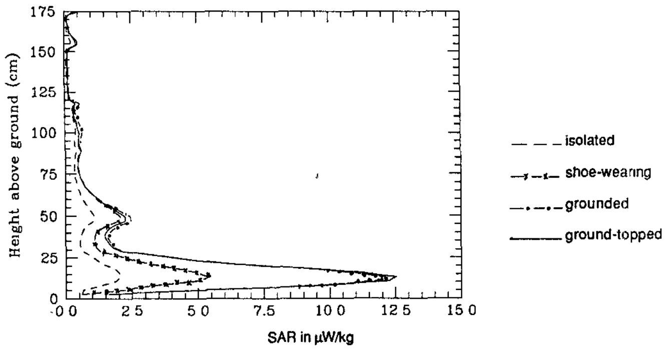

Fig. 6. Layer-averaged SAR distributions for an isolated, shoe-wearing, grounded, and ground-topped man model at 40.68 MHz under near-field exposure condition. Maximum $E_{\text{rms}}=1$ V/m at 21 cm in front of the parallel-plate applicator.

TABLE II
THE WHOLE-BODY-AVERAGED SAR'S FOR THE MAN MODEL FOR THE VARIOUS EXPOSURE CONDITIONS: ISOLATED, SHOE-WEARING, GROUNDED, BOTTOM GROUND, AND A GROUNDED TOP PLATE 13.1 cm ABOVE THE HEAD. A SPATIALLY MAXIMUM, VERTICAL E FIELD OF 1 V/m (rms) IS ASSUMED INCIDENT ON THE MODEL.

	SARs in μW/kg Condition of exposure for the model			
Frequency	Isolated	Shoe-Wearing	Grounded	With grounded top plate
27 12 MHz	0.119	0 180	0.245	0.263
40 68 MHz	0.322	0.638	0.698	0 754

Torso section
Layer #37 of Fig.1

				327	329				
			309	250	219	378			
			55	281	271	297			
			51	224	207	274			
				437	207	195	256		
			523	331	182	89	177	138	205
		95	349	291	165	125	223	184	74
		2	196	155	51	143	222	195	70
		32	113	155	107	78	125	158	80
	231	89	151	101	132	69	45	84	81
Front	146	91	131	101	109	77	47	85	75
	543	48	160	137	178	100	76	173	96
		20	157	156	104	100	226	182	116
		3	329	237	82	156	278	174	158
			514	368	194	81	176	156	217
				439	233	254	370		
			49	274	286	319			
			68	303	275	282			
			383	258	213	352			
				385	360				

Knee section
Layer #19 of Fig.1

		964	836	919	1305	
	64	451	165	188	805	1561
	72	455	248	218	896	1776
		1272	1029	581	793	2066
				2275	2432	
Front						
				1964	2101	
		1151	1105	629	829	2144
	55	504	248	217	904	1773
	80	445	182	202	802	1537
		1136	797	876	1280	

Ankle section
Layer #4 of Fig.1

	3827	5732	6593	
	3186	1460	3380	7654
	4191	2628	3211	8060
Front				
	3707	2386	2915	6815
	3037	1310	3173	7267
	3927	5375	6135	

Fig. 7. SAR distribution in nW/kg for ankle and knee sections and for the section of the torso in front of the parallel-plate applicator for grounded condition of the model. Frequency = 27.12 MHz; $E_{\text{peak}} =$ 1 V/m (rms).

Torso section
Layer #37 of Fig.1

				1077	1002				
			1257	859	747	1172			
			192	946	919	981			
			267	743	686	708			
				1213	634	597	766		
			1155	937	551	281	568	424	636
		319	805	811	513	392	726	598	235
		12	464	437	151	461	740	647	221
		48	271	450	333	257	424	530	260
	799	149	363	291	418	236	154	279	263
Front	520	157	302	291	347	295	158	284	244
	867	83	378	381	565	339	253	581	316
		33	382	464	322	329	746	610	384
		51	776	661	258	499	927	564	515
			1149	1051	589	256	576	494	691
				1211	718	602	845		
			212	876	713	870			
			210	999	929	951			
			1178	879	732	1125			
				1273	1175				

Knee section
Layer #19 of Fig.1

		2986	2492	2897	4119	
	204	1393	486	658	2622	5053
	215	1394	746	755	2945	5850
		3971	3194	1881	2623	7040
				7741	8347	
Front						
				6340	7511	
		3585	3416	2051	2784	7364
	230	1549	754	765	3021	5955
	282	1394	538	716	2664	5088
		3513	2425	2833	4132	

Ankle section
Layer #4 of Fig.1

	11240	18899	21417	
	10592	4940	11670	25483
	13796	8938	10680	32964
Front				
	12463	8245	9830	31888
	10239	4505	11144	24813
	12848	18163	20426	

Fig. 8. SAR distribution in nW/kg for ankle and knee sections and for the section of the torso in front of the parallel-plate applicator for grounded condition of the model. Frequency = 40.68 MHz; $E_{\text{peak}} =$ 1 V/m (rms).

91.4 percent of those calculated for the grounded condition at 27.12 and 40.68 MHz, respectively. It is interesting to note from Figs. 5 and 6 that the highest layer-averaged SAR's are calculated for the sections of the body corresponding to the knee and the ankle, respectively, even though these parts of the human anatomy are located in regions of lower incident fields (see Figs. 2 and 3). The reason for higher *SAR*'s for the knee and ankle sections is, of course, the high amount of bone content which forces the induced currents to flow through relatively small conducting sectional areas, thereby giving high current densities and hence high *SAR*'s. A similar phenomenon has been previously reported for plane-wave irradiation conditions [5]. The *SAR* distributions for the ankle and knee sections as well as the section of the torso directly in front of the applicator are shown in Figs. 7 and 8, respectively, for the grounded condition of the model for irradiation frequencies of 27.12 and 40.68 MHz.

We have used the internal E fields to calculate the local current densities from the relationship

$$\vec{J} = \sum_{x,y,z} (\sigma_x + j\omega\epsilon_x)E_x. \tag{2}$$

Figs. 9 and 10 show the x-, y-, and z-directed currents for the various sections of the body that are obtained by summing up the individual current $\vec{J}\delta^2$ for each of the cells. Since the vertical current is by far the largest of the three components, the calculated vertical current distributions are shown as a function of height in Figs. 11 and 12 for the various conditions of irradiation, identified earlier

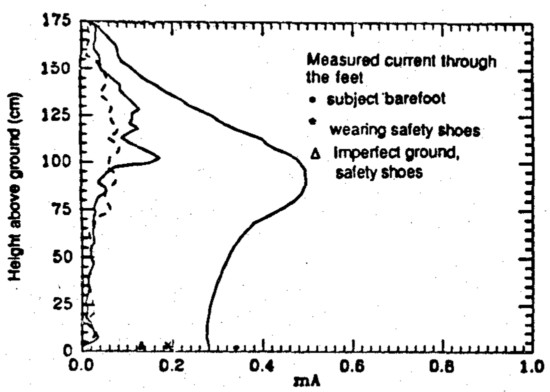

Fig. 9. Induced vertical and horizontal current distributions for a grounded man model at 27.12 MHz under near-field exposure condition. The maximum $E_{\rm rms} = 1$ V/m at 21 cm in front of the parallel-plate applicator. Dashed line: horizontal currents I_x; continuous line (left): horizontal current I_y; continuous line (right): vertical current I_z.

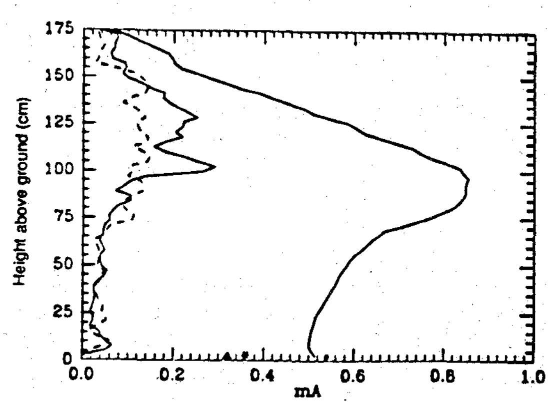

Fig. 10. Induced vertical and horizontal current distributions for a grounded man model at 40.68 MHz under near-field exposure condition. The maximum $E_{\rm rms} = 1$ V/m at 21 cm in front of the parallel-plate applicator. Dashed line: horizontal currents I_x; continuous line (left): horizontal current I_y; continuous line (right): vertical current I_z.

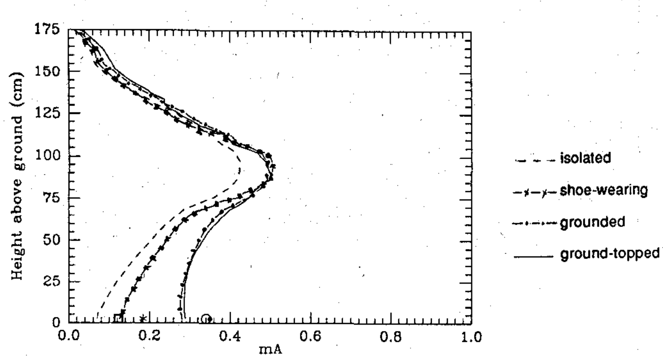

Fig. 11. Induced vertical current distributions for an isolated, shoe-wearing, grounded, and ground-topped man model at 27.12 MHz under near-field exposure condition. The maximum $E_{\rm rms} = 1$ V/m at 21 cm in front of the parallel-plate applicator. Measured foot currents for a human subject: isolated (□), rubber-soled shoes (∗), barefoot grounded (○), and ground-topped (●).

in Figs. 5 and 6. Torso currents as high as 0.5 and 0.86 mA/(V/m) have been calculated for irradiation frequencies of 27.12 and 40.68 MHz, respectively. Since peak E fields as high as 1000–2700 V/m have been measured at locations typically occupied by the operator, significant internal RF currents on the order of 0.5–2.3 A are projected for the operators.

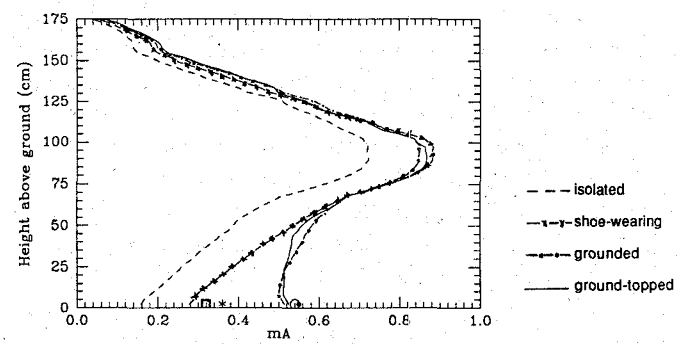

Fig. 12. Induced vertical current distributions for an isolated, shoe-wearing, grounded, and ground-topped man model at 40.68 MHz under near-field exposure condition. The maximum $E_{\rm rms} = 1$ V/m at 21 cm in front of the parallel-plate applicator. Measured foot currents for a human subject: isolated (□), rubber-soled shoes (∗), barefoot grounded (○), and ground-topped (●).

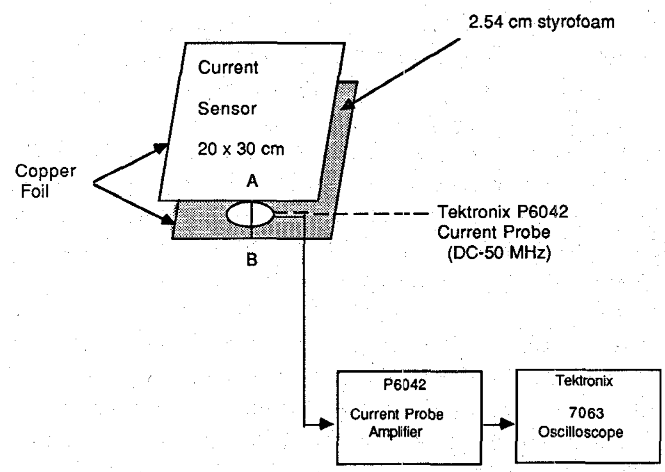

Fig. 13. Block diagram of the induced RF current measurement system.

Since foot currents can be measured for a human subject, we have also compared a few of the calculated values with the values that were measured for the leakage fields of a parallel-plate applicator of dimensions used for the calculations (plate dimensions 57.64×15.74 cm; interplate separation = 2.62 cm). The current sensor and measurement system used for these measurements is shown in Fig. 13. Even though this measurement system is somewhat different than that previously described in [5], the logic is still the same. As in [5], the RF power to the parallel plates of the applicator (Fig. 1.) is provided using an MCL model 15122 power generator. The electric field intensity at the intended position of the subject is measured using Holaday Industries model 3003 probe. The subject stands on the upper plate A of the bilayer sensor (Fig. 13) so that the separation between the front of the torso to the applicator aperture is 21 cm. The current passing from the feet of a 1.72-m-tall subject through the current sensor to ground is measured by means of a Tektronix model P6042 current probe which loops around the current carrying wire AB (2 mm diameter) in Fig. 13. For grounded conditions, the ground plane underneath the current sensor is provided by a 1/16-in-thick aluminum plate of dimensions 1.2×2.4 m^2. The foot currents have been measured for grounded conditions and for a subject wearing electrical "safety shoes" (size 11, Vibram Manufacturing Company, 1.75-cm rubber sole thickness) as well as for conditions where the aluminum grounding plate was removed and the current sensor was placed on the vinyl-covered floor. For the so-called isolated condition, the foot currents were measured by using a sufficient styrofoam thickness (typically larger than 12.7 cm) under the feet to "isolate" the subject from ground. For such thicknesses the currents were found to be independent of styrofoam thickness. The measured currents for these conditions are shown for comparison in Figs. 9–12 for the corresponding irradiation frequencies. The results are in reasonable agreement with the calculated values.

V. Conclusions

We have used an anatomically based 5628-cell model of man to calculate local, layer-averaged, and whole-body-averaged *SAR*'s and internal RF currents at 27.12 and 40.68 MHz for spatially variable electromagnetic fields of a parallel-plate applicator representative of RF dielectric heaters used in industry. The conditions of exposure of the man model considered are: isolated from ground, shoe-wearing condition, feet in contact with ground, and an additional grounded top plate 13.1 cm above the head to simulate screen rooms that are occasionally used for RF heaters.

Since peak E fields as high as 1000–2700 V/m have been measured at locations typically occupied by the operator, significant internal RF currents on the order of 0.5–2.3 A are projected for the operators. Measurements of the foot currents at 27.12 and 40.68 MHz for a human subject are in reasonable agreement with the calculated values for the various conditions of exposure.

References

[1] "Study of radio-frequency and microwave radiation (Phase I)," Final Rep. prepared for OSHA by Centaur Assoc., Inc., Washington, DC, 1982.

[2] D. L. Conover, W. E. Murray, Jr., E. D. Foley, J. M. Lary, and W. H. Parr, "Measurement of electric- and magnetic-field strengths from industrial radio-frequency (6-38 MHz) plastic sealers," *Proc. IEEE*, vol. 68, pp. 17–20, 1980.

[3] M. A. Stuchly, M. H. Repacholi, D. Lecuyer, and R. Mann, "Radiation survey of dielectric RF heaters in Canada," *J. Microwave Power*, vol. 15, pp. 113–121, 1980.

[4] I. Chatterjee, M. J. Hagmann, and O. P. Gandhi, "Electromagnetic-energy deposition in an inhomogeneous block model of man for near-field irradiation conditions," *IEEE Trans. Microwave Theory Tech.*, vol. MTT-28, pp. 1452–1459, 1980.

[5] O. P. Gandhi, J-Y Chen, and A. Riazi, "Currents induced in a human being for plane-wave exposure conditions, 0-50 MHz and for RF sealers," *IEEE Trans. Biomed. Eng.*, vol. BME-33, pp. 757–767, 1986.

[6] D. M. Sullivan, D. T. Borup, and O. P. Gandhi, "Use of the finite-difference time-domain method in calculating EM absorption in human tissues," *IEEE Trans. Biomed. Eng.*, vol. BME-34, pp. 148–157, 1987.

[7] D. M. Sullivan, O. P. Gandhi, and A. Taflove, "Use of the finite-difference time-domain method for calculating EM absorption in man models," *IEEE Trans. Biomed. Eng.*, vol. 35, pp. 179–186, Mar. 1988.

[8] C-Q. Wang and O. P. Gandhi, "Numerical simulation of annual-phased arrays for anatomically based models using the FDTD method," pp. 118–126, this issue.

[9] K. S. Yee, "Numerical solution of initial boundary value problems involving Maxwell's equations in isotropic media," *IEEE Trans. Antennas Propagat.*, vol. AP-14, pp. 302–307, 1966.

[10] A. Taflove and M. E. Brodwin, "Computation of electromagnetic fields and induced temperatures within a model of the microwave-irradiated human eye," *IEEE Trans. Microwave Theory Tech.*, vol. MTT-23, pp. 888–896, 1975.

[11] A. Taflove, "Application of the finite-difference time-domain method to sinusoidal steady-state electromagnetic-penetration problems, *IEEE Trans. Electromagn. Compat.*, vol. EMC-22, pp. 191–202, 1980.

[12] K. Umashankar and A. Taflove, "A novel method to analyze electromagnetic scattering of complex objects," *IEEE Trans. Electromagn. Compat.*, vol. EMC-24, pp. 397–405, 1982.

[13] R. Holland, "THREDE: A free-field EMP coupling and scattering code," *IEEE Trans. Nucl. Sci.*, vol. NS-24, pp. 2416–2421, 1977.

[14] K. S. Kunz and K-M Lee, "A three-dimensional finite-difference solution of the external response of an aircraft to a complex transient EM environment: Part 1—The method and its implementation," *IEEE Trans. Electromagn. Compat.*, vol. EMC-20, pp. 328–332, 1978.

[15] A. C. Eycleshymer and D. M. Schoemaker, *A Cross-Section Anatomy*. New York, London: Appleton, 1911.

[16] M. A. Stuchly and S. S. Stuchly, "Dielectric properties of biological substances—Tabulated," *J. Microwave Power*, vol. 15, pp. 19–26, 1980.

[17] C. C. Johnson and A. W. Guy, "Nonionizing electromagnetic wave effects in biological materials and systems," *Proc. IEEE*, vol. 60, pp. 692–720, 1972.

Jin-Yuan Chen (S'88) was born in Jiangsu, China, in 1945. He received B.S. and M.S. degrees in electrical engineering from the University of Science and Technology of China (USTC) in 1970 and 1981, respectively. He is now a Ph.D. candidate in the Department of Electrical Engineering, University of Utah, Salt Lake City, where he is currently involved in bioelectromagnetics.

From 1970 to 1978 and from 1981 to 1983 he served as a Teacher and an Instructor in the Department of Electrical Engineering at USTC. At the same time, he studied the frequency synthesizer, the measurement of high stability and high accuracy frequency sources, the high stability centimeter-wave, millimeter-wave frequency source, the phase-locked millimeter-wave transmitter, the tracking and phase-locked millimeter-wave Doppler receiver, and the new millimeter-wave Gunn oscillator phase-locking method.

Mr. Chen was awarded the Guo Mou-ruo prize and the science research prizes of the Chinese Academy of Sciences in 1981, 1982 and 1983, respectively, for his excellent research. He recently received the best student paper awards for both platform and poster papers at the 10th Annual Meeting of the Bioelectromagnetics Society, Stamford, CT, 1988.

Om P. Gandhi (S'57–M'58–SM'65–F'79) is a Professor of Electrical Engineering at the University of Utah, Salt Lake City. He is the author or coauthor of several book chapters, over 200 journal articles on microwave tubes, solid-state devices, and electromagnetic dosimetry and the textbook *Microwave Engineering and Applications* (New York: Pergamon).

Dr. Gandhi received the Distinguished Research Award from the University of Utah for 1979–1980 and a special award for "Outstanding Technical Achievement" from the IEEE, Utah Section, in 1975. He is Cochairman of the ANSI C95.4 Subcommittee on the RF Safety Standards (1988–) and a past Chairman of the IEEE Committee on Man and Radiation (COMAR). His name is listed in *Who's Who in the World*, *Who's Who in America*, *Who's Who in Engineering*, and *Who's Who in Technology Today*.